

Light Response of Three Water-Soluble Mn^I PhotoCORMs: Spectroscopic Features and CO Release Investigation

Vitor C. Weiss,^{a,b} André L. Amorim,^a Fernando R. Xavier,^c Adailton J. Bortoluzzi,^a Ademir Neves^a and Rosely A. Peralta^{✉*,a}

^aLaboratório de Bioinorgânica e Cristalografia (LABINC), Departamento de Química, Universidade Federal de Santa Catarina, 88040-900 Florianópolis-SC, Brazil

^bInstituto Federal de Educação, Ciência e Tecnologia de Santa Catarina (IFSC), Campus Florianópolis, 88020-300 Florianópolis-SC, Brazil

^cUniversidade do Estado de Santa Catarina (UDESC), Campus Joinville, 89219-710 Joinville-SC, Brazil

Currently, there is great interest in the study of water-soluble metal compounds capable of releasing carbon monoxide, due to their potential therapeutic use. This paper reports the synthesis, spectroscopic characteristics and CO release properties of three water-soluble manganese(I) carbonyl compounds [Mn(aaz)(CO)₃]Br (**1**; where aaz = 6-amino-6-methylperhydro-1,4-diazepine), [Mn(Me₂aaz)(CO)₃]Br (**2**; where Me₂aaz = 6-amino-1,4,6-trimethyl-1,4-diazacycloheptane) and [Mn(tacn)(CO)₃]Br (**3**; where tacn = 1,4,7-triazacyclononane), that can act as photoCORMs (where CORM is carbon monoxide-releasing molecule). The main aim was to propose a mechanism for the CO release. Compounds **1-3** are capable of releasing carbon monoxide when exposed to light (λ_{385} and λ_{410}) and thus, act as photoCORMs. The formation of a biscarbonyl intermediate was identified during the photo-release process at λ_{385} and the quantum yields and rates of CO release were determined. The proposed CO release mechanisms involve two steps, where photo and redox processes take place, and compounds **1** and **2** exhibit a slightly different mechanism from compound **3**. A good understanding of the CO photo-release mechanism is very important with regard to the development of more efficient compounds, particularly those intended for medical applications.

Keywords: photoCORM, manganese(I) tricarbonyl compounds, photoreactivity

Introduction

Carbon monoxide (CO) is widely known as a silent killer, but the discovery of its beneficial features has led several research groups to use CO as a therapeutic agent in the past decade.^{1,2} Since it is a cell signaling molecule,^{3,4} the therapeutic properties of carbon monoxide range from anti-inflammatory and antiapoptotic to having an antiproliferation effect on malign cells.⁵⁻⁷ However, the direct application of gaseous CO as a therapeutic agent has two major drawbacks: its high affinity towards hemoglobin⁸ and the uncertainties associated with its direct inhalation by patients,^{9,10} given a lack of control and specificity. One way to overcome these disadvantages is the use of molecular carriers, which act as prodrugs and can transport carbon monoxide into the organism in a

controlled manner, only releasing CO under the influence of a specific trigger.¹¹⁻¹³

Several carriers based on organic compounds^{14,15} or using transition metals, such as tungsten, molybdenum, iron, ruthenium, rhenium and manganese,¹⁶⁻²¹ have been used to deliver CO to the organism, the latter being preferred due to the high flexibility in terms of the properties obtained from both the metal center and the organic framework.¹³ The correct selection of these properties is essential in the development of new metal carbonyl compounds (MCCs),¹² which should preferentially be water soluble.^{22,23}

Among the first CO-releasing molecules are those that release carbon monoxide upon ligand exchange between the carbonyl in the first coordination sphere of the MCC and a coordinating species present in the medium studied. In the case of carbon monoxide-releasing molecule (CORM)-3, for instance, the CO release mechanism is highly dependent on the medium.²⁴

*e-mail: rosely.peralta@ufsc.br

Photoactivation of the MCCs seems to be the most attractive trigger, considering the temporal and spatial control of the carbon monoxide release. Metal carbonyl compounds such as these, which are of great importance, are termed photoCORMs.^{25,26}

In this regard, several research groups have been studying photoCORMs. They present a wide array of characteristics, such as the lipophilic properties of CORM-1 (Mn₂(CO)₁₀)²⁷ and the localization of the prodrug, which can be performed by Raman microspectroscopy in the case of [Mn(tmp)(CO)₃]⁺ (tmp: tris((pyrazolyl)methane)²⁸ or fluorescence microscopy for [Mn(Imdansyl)(CO)₃(phen)](CF₃SO₃)²⁹ (Imdansyl: dansylimidazole).

Despite the recent advances, the CO release mechanism associated with manganese photoCORMs, which have more than one carbonyl group in the first coordination sphere, are not commonly explored in depth, one counterexample being the studies conducted by the Kurz and co-workers.^{30,31} In this context, we report herein three new manganese photoCORMs that show desirable properties as carbonyl-containing prodrugs, such as high stability and water solubility, as well as some mechanistic insights regarding the carbon monoxide release process.

The synthesis and characterization of the three carbonyl compounds mentioned above, [Mn(aaz)(CO)₃]Br (1; where aaz = 6-amino-6-methylperhydro-1,4-diazepine), [Mn(Me₂aaz)(CO)₃]Br (2; where Me₂aaz = 6-amino-1,4,6-trimethyl-1,4-diazacycloheptane) and [Mn(tacn)(CO)₃]Br (3; where tacn = 1,4,7-triazacyclononane) (Figure 1) are reported herein. All compounds were fully characterized using standard techniques including infrared (IR), ultraviolet-visible (UV-Vis) and nuclear magnetic resonance (NMR) spectroscopies, electrochemistry, X-ray crystallography and electrospray ionization-mass spectrometry (ESI-MS). The stability and the CO release were monitored, using an array of techniques, and the mechanisms for the CO release are proposed.

Experimental

General procedures

All solvents were dried with molecular sieves (4 Å) for 72 h prior to use unless otherwise specified. The solutions

were degassed either by freeze pump thaw cycles or by argon flux. The ligands aaz and Me₂aaz were synthesized analogously to previous published procedures,^{32,33} while tacn was bought from Sigma-Aldrich (São Paulo, Brazil) and used without further purification. The [Mn(CO)₅Br] and lyophilized human hemoglobin were purchased from Sigma-Aldrich (São Paulo, Brazil).

Physical measurements

Elemental analysis was performed on a PerkinElmer (Model 2400 Series II) CHNS/O analyzer coupled with a PerkinElmer scale (Model Autobalance AD 6000) using 5.0 grade helium and 6.0 grade oxygen. The infrared spectra were obtained on a PerkinElmer Spectrum 100 FT-IR spectrophotometer in the range of 4000 to 450 cm⁻¹. The solid samples were analyzed by attenuated total reflectance (ATR) using the UATR module and the solubilized samples were homogenized with dried KBr powder. NMR spectroscopy was carried out on a Bruker Ascend400 Varian FT-NMR 400 MHz setup using dimethyl sulfoxide (DMSO-*d*₆) as the solvent, at 25 °C. Chemical shifts were referenced to tetramethylsilane (TMS, δ 0.000 ppm). For the kinetic experiments, ¹H NMR data were acquired at selected time intervals during 1 h of light irradiation at 385 nm. ESI-MS was performed on an Amazon-Ions Trap MS system in spectroscopic grade acetonitrile solution with an approximate concentration of 500 ppb and estimated flow of 180 μL min⁻¹. The temperature of the capillary was maintained at 180-200 °C and the capillary voltage was between -400 and -500 V. The redox behavior of the title compounds was investigated by cyclic and square wave voltammetry using a BAS model Epsilon potentiostat (Bioanalytical Systems, Inc.) in spectroscopic grade acetonitrile with concentrations of 1.00 × 10⁻⁴ mol L⁻¹, under argon atmosphere. Tetrabutylammonium hexafluorophosphate (TBAPF₆) with a concentration of 0.1 mol L⁻¹ was used as the supporting electrolyte. The following electrodes were used: Ag/Ag⁺ (reference) and platinum (work and auxiliary). The ferrocene/ferrocenium pair (Fc/Fc⁺) was used as an internal reference and the potentials were referenced *versus* the normal hydrogen electrode (NHE).³⁴

Further details on the single crystal X-ray diffraction (XRD) analysis, density functional theory (DFT) and

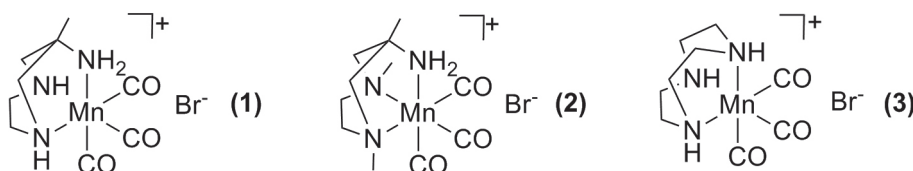


Figure 1. Schematic representation of the manganese(I) carbonyl compounds: [Mn(aaz)(CO)₃]Br (1); [Mn(Me₂aaz)(CO)₃]Br (2) and [Mn(tacn)(CO)₃]Br (3).

time-dependent density functional theory (TD-DFT) calculations, CO release and hemoglobin assay are provided in the Supplementary Information.

CO release assay

To determine the stability of the organometallic compounds, the charge transfer bands were monitored over a 14-h period in the absence of light. The compounds were solubilized in H₂O with concentrations of 1.00×10^{-3} mol L⁻¹ and subsequently diluted to 6.00×10^{-4} mol L⁻¹.

After investigating the stability in solution, the quantum yield of CO release was determined by monitoring the decrease of the charge transfer band, at around 300 and 400 nm. The ferrioxalate actinometry assay¹⁹ was used to determine the photo flow of the light source used.

The light sources employed to perform the CO release assays were two sets of light emitting diodes (LEDs), with the following wavelengths: $\lambda_{385} = 385 \pm 10$ nm (photon flux = 1.13×10^{-8} Einstein s⁻¹) and $\lambda_{410} = 410 \pm 5$ nm (photon flux = 1.03×10^{-8} Einstein s⁻¹). The distance between the analyte and the lamp was set at 3.0 cm, where the light source was arranged perpendicularly to the sample.

Hemoglobin assay

A modified version of the deoxymyoglobin assay was conducted,³⁵ using hemoglobin as the substrate. A stock solution of hemoglobin with a concentration of approximately 3.00×10^{-5} mol L⁻¹ (2 mg, 2 mL) was prepared by dissolving the protein in a degassed phosphate buffer saline (PBS) solution (0.1 mol L⁻¹, pH 7.4) to which sodium dithionite was added (20 mg). The organometallic compounds were dissolved in water, resulting in concentrations of 2.57×10^{-4} mol L⁻¹. The measurements were performed by diluting 146 μ L of the MCC solution in 1 mL of the hemoglobin solution. The cuvettes were sealed with a Teflon stopper, preventing the loss of carbon monoxide. The samples were irradiated identically to the CO release assay reported previously but using only the λ_{385} LED. In order to detect the influence of sodium dithionite on the carbon monoxide release, the samples were also analyzed without the incidence of light. The formation of HbCO was monitored until no further spectral changes were observed, and the amount of CO released was calculated, taking into consideration that Hb is a tetramer.

Synthesis of the complexes

All photoCORMs studied were synthesized using the standard Schlenk technique by adding [Mn(CO)₅Br]

(0.3 mmol, 82.4 mg, 1 equiv.) to a frozen CH₃CN solution (10 mL) of the ligands (0.3 mmol, 38.7 mg (aaz or tacn) and 47.1 mg (Me₂aaz), 1 equiv.). After reaching ambient temperature the resulting solution was refluxed for 12 h under inert atmosphere and dim light conditions. After this time, the resulting mixtures were cooled to room temperature and the precipitates were collected by vacuum filtration and washed three times with cold CH₂Cl₂, resulting in pale yellow powders. Yellow crystals of **1** and **3** were obtained by slow evaporation from ethanol solutions at 20 °C. Good quality crystals of [Mn(Me₂aaz)(CO)₃]⁺ could only be obtained by exchanging the bromide counterion for nitrate, by adding one equivalent of AgNO₃ to an acetonitrile solution of **2**, the silver bromide formed was filtered and the solution left to stand at room temperature, and yellow crystals were obtained.

[Mn(aaz)(CO)₃]Br (**1**)

Pale yellow solid, yield 68%: 70.78 mg; 346.97 g mol⁻¹; IR (ATR) ν / cm⁻¹ 3335, 3192, 3097, 2024, 1879; UV (H₂O) λ_{max} / nm and its respective ϵ / (L mol⁻¹ cm⁻¹) 349 (1317); HRMS (Fourier transform mass spectrometry (FTMS) + pESI) m/z , calcd. for C₉H₁₅BrMnN₃O₃ [M]⁺: 268.0448, found: 268.3712; elemental analysis (C₉H₁₅BrMnN₃O₃), found (calculated): C, 30.35 (31.06); H, 4.39 (4.34); N, 11.74 (12.07); ¹H NMR (400 MHz, DMSO-*d*₆) δ 1.07 (s, 3H, CH₃), 2.30-2.40 (m, 2H, CH₂), 2.65-2.78 (m, 2H, CH₂), 2.88-2.98 (m, 2H, CH₂), 3.21 (m, 2H, CH₂), 4.54 (s, 2H, NH₂), 6.24 (s, 2H, NH); ¹³C NMR (100 MHz, DMSO-*d*₆) δ 19.7, 54.1, 58.0, 61.5.

[Mn(Me₂aaz)(CO)₃]Br (**2**)

Pale yellow solid, yield 70%: 78.98 mg; 376.13 g mol⁻¹; IR (ATR) ν / cm⁻¹ 3168, 2962, 2882, 2020, 1893; UV (H₂O) λ_{max} / nm and its respective ϵ / (L mol⁻¹ cm⁻¹) 354 (1368); HRMS (FTMS + pESI) m/z , calcd. for C₁₁H₁₉BrMnN₃O₃ [M]⁺: 296.0817, found: 296.2500; elemental analysis (C₁₁H₁₉BrMnN₃O₃), found (calculated): C, 34.79 (35.13); H, 5.27 (5.09); N, 11.45 (11.17); ¹H NMR (400 MHz, DMSO-*d*₆) δ 1.11 (s, 3H, CH₃), 2.59-2.72 (m, 2H, CH₂), 2.72-2.86 (m, 2H, CH₂), 2.96 (s, 3H, CH₃), 2.99-3.08 (m, 2H, CH₂), 5.05 (s, 2H, NH₂); ¹³C NMR (100 MHz, DMSO-*d*₆) δ 20.0, 56.5, 58.9, 64.0, 70.6, 219.4.

[Mn(tacn)(CO)₃]Br (**3**)

Pale yellow solid, yield 71%: 73.9 mg; 346.97 g mol⁻¹; IR (ATR) ν / cm⁻¹ 3114, 2952, 2886, 2019, 1870; UV (H₂O) λ_{max} / nm and its respective ϵ / (L mol⁻¹ cm⁻¹) 344 (1102); HRMS (FTMS + pESI) m/z , calcd. for C₉H₁₅BrMnN₃O₃ [M]⁺: 268.0448, found: 267.5568; elemental analysis (C₉H₁₅BrMnN₃O₃), found (calculated): C, 30.53 (31.06);

H, 4.28 (4.34); N, 11.58 (12.07); ¹H NMR (400 MHz, DMSO-*d*₆) δ 2.57-2.74 (m, 6H, CH₂), 2.81-2.98 (m, 6H, CH₂), 6.71 (s, 3H, NH); ¹³C NMR (100 MHz, DMSO-*d*₆) δ 49.7, 220.9.

Results and Discussion

Solid state characterization

In order to avoid oxidation of the Mn^I ion we performed the syntheses with extended reaction times in dry, degassed solvent, as described in the Experimental section. With this approach and after recrystallization in adequate solvent, single crystals, suitable for X-ray analysis, were obtained for all compounds.

The molecular arrangements for compounds **1**, **2** and **3** are shown in Figure 2. As expected, all structures have distorted octahedral coordination geometry, with the nitrogen-rich ligands presenting a facial coordination mode. Compound **1** crystallizes in a monoclinic system and *P*2₁/*c* spatial group whereas compounds **2** and **3** crystallize in the orthorhombic space groups *Pna*21 and *Pbca*, respectively. The bond angles show larger distortions for **1** and **2**, as a direct result of the aaz and Me₂aaz ligands. These ligands have more conformational freedom when compared to the tacn used for **3**, resulting in more differentiated bond angles (Table 1). The Mn1–C bonds are shorter than Mn1–N bonds due the strong π-back-bonding effect between these atoms which increases the distortion in the octahedral geometry. In the structures of compounds **1** and **2** the Mn1–N1 bond distances (2.068(3) Å for **1** and 2.046(4) Å for **2**) are shorter than the Mn1–N2 (2.097(3) Å for **1** and 2.110(6) Å for **2**) and Mn1–N3 (2.098(3) Å for **1** and 2.109(5) Å for **2**) bonds thereto. This occurs because the amine nitrogen N1 is positioned outside the chelate ring of these ligands which gives it greater conformational freedom and interaction with the metal center of Mn1. Consequently, the Mn1–C1 binding lengths for these two compounds, 1.804(4) Å for **1** and 1.793(6) Å for **2** are slightly shorter than Mn1–C2 (1.809(4) Å for **1** and 1.801(7) Å for **2**) and Mn1–C3 (1.806(4) Å for **1** and 1.811(7) Å for **2**) due to the *trans*-influence. As the N1 atom is closer to the metal center it increases the electron density on it resulting in a higher π-back-bonding between the Mn1–C1 atoms in comparison to Mn1–C2 and Mn1–C3 atoms for **1** and **2**. On the other hand, for compound **3** all Mn1–N bonding distances are very similar since the tacn is a symmetrical macrocyclic ligand. Furthermore, compounds **1-3** present bond angles and bond lengths which are comparable to Mn^I tricarbonyl compounds with nitrogen chelating ligands already reported in the literature, for example [Mn(CO)₃(*k*³-tpa)]⁺.³¹

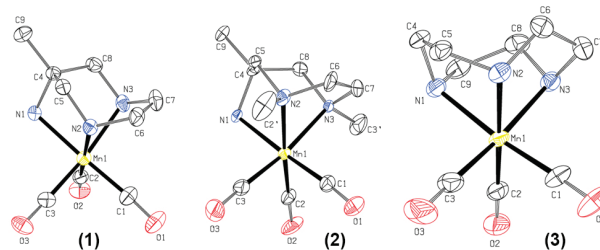


Figure 2. Molecular structure of cation complexes **1-3** from left to right, hydrogen and counter-ions are omitted for clarity. Thermal ellipsoids are shown at 50% probability level.

Table 1. Selected bond lengths and angles of **1-3**

	1	2	3	
Bond length / Å	Mn1–C1	1.804(4)	1.793(6)	1.809(3)
	Mn1–C2	1.809(4)	1.801(7)	1.814(3)
	Mn1–C3	1.806(4)	1.811(7)	1.802(3)
	Mn1–N1	2.068(3)	2.046(4)	2.074(2)
	Mn1–N2	2.097(3)	2.110(6)	2.069(2)
	Mn1–N3	2.098(3)	2.109(5)	2.071(2)
Bond angle / degree	C1–Mn1–C2	86.22(16)	88.2(3)	90.02(12)
	C1–Mn1–C3	90.11(18)	89.8(3)	88.95(14)
	C2–Mn1–C3	92.09(15)	89.3(4)	90.11(13)
	N1–Mn1–N2	81.15(10)	82.3(2)	81.19(8)
	N1–Mn1–N3	82.33(11)	81.93(19)	81.12(8)
	N2–Mn1–N3	74.58(11)	76.6(2)	80.88(8)

The infrared spectra of the ligands and the complexes show the coordination between the metal ions and the ligands through the amine nitrogen. The bands characteristic of the NH and NH₂ groups appear in the region of 3300 to 3400 cm⁻¹ for the free ligands, whereas for compounds **1-3** this band is shifted to the lower energy region, indicating coordination of the ligand to the metal ion through the nitrogen.

The infrared results also corroborate the facial ligand arrangement, since their symmetry resembles that of a *C*_{3v} point group, displaying two intense vibrational stretching bands, at around 2100 and 1800 cm⁻¹. The former is associated with the symmetrical CO stretching and the latter is attributed to the two degenerate asymmetrical CO stretching bands, which are directly influenced by the symmetry of the ligands. As an example, compound **3**, which shows the most symmetry, displays high degeneracy of the asymmetrical band. In contrast, upon increasing the asymmetry from **1** to **2** the asymmetrical bands tend to split, forming three CO stretching bands (Figures S1-S3, Supplementary Information (SI) section).

Identification of the initial species in solution

Besides the solid-state characterization, the stability of the title compounds was assessed in water and acetonitrile

solutions. All compounds have high stability in both media in the dark, showing only slight changes of the absorption spectra over a period of 14 h (Figure S4, SI section). Complexes **1** and **2** showed less than 3% of spectral variation while complex **3** remained practically unchanged. Furthermore, the ESI-MS analysis conducted in acetonitrile confirms the stability of **1-3** in the dark, since the compounds do not exhibit CO release during the analysis, where the molecular ion is the base peak (Figures S5-S7, SI section).

The absorption spectra of **1**, **2** and **3** in water show intense bands at 350, 355 and 346 nm, respectively, and a minor shoulder at around 268 nm (Figure 3a), which

are in agreement with the theoretical values. The analysis of the calculated excitations indicates that the lower energy band has two major transitions (Figure 4) and the higher energy band has three major transitions, both associated with excitations of the Mn^I *d* to the $p\pi^*$ nitrogen orbitals. The superposition of the theoretical spectra with the experimental results showed good agreement (Figures 3b-3d).

TD-DFT calculations with the conductor-like polarizable continuum model (CPCM) solvation model on the optimized ground states of **1-3** revealed that the orbitals of both absorptions have major contributions from the highest occupied molecular orbitals (HOMOs), which

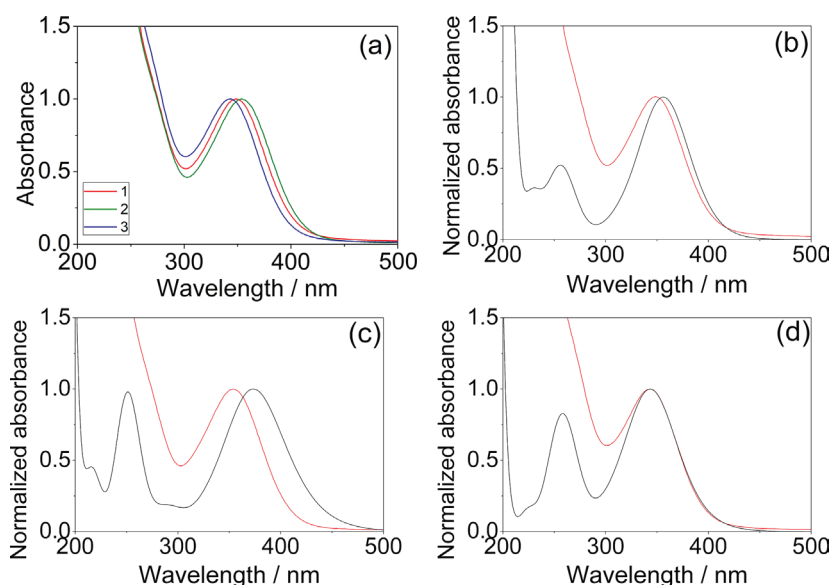


Figure 3. (a) Absorption spectra of **1-3** in aqueous solution; (b, c, d) superposed absorption spectra (red dashed line) and theoretical values (black line) for **1-3**, respectively, obtained from plotting a Gaussian distribution with $\sigma = 0.3$ eV over the twenty most prominent calculated excitations.

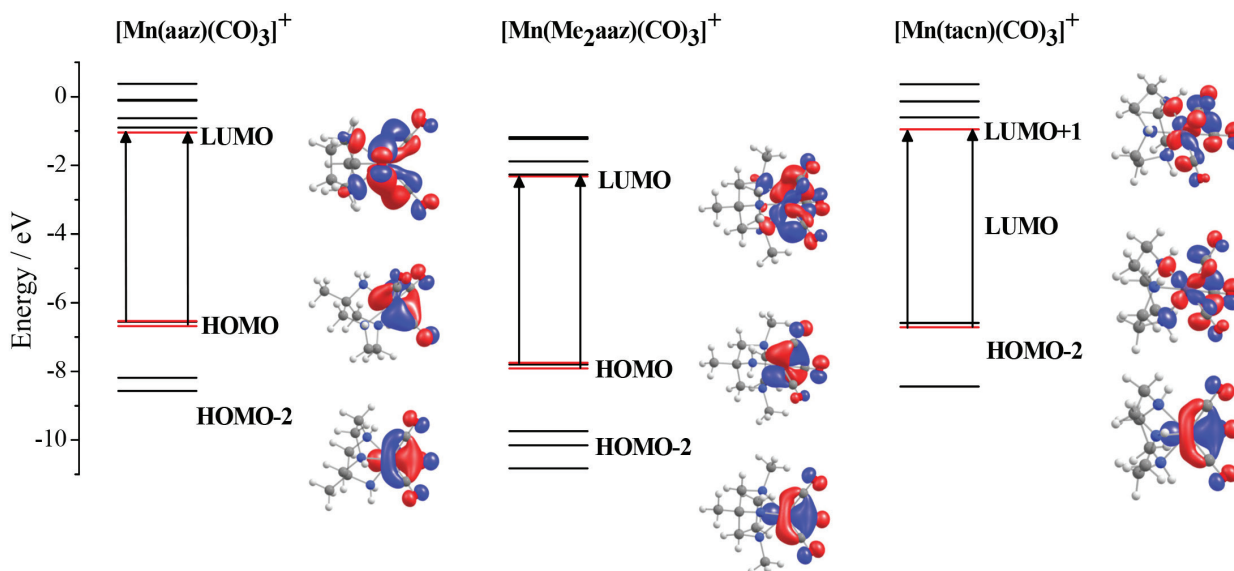


Figure 4. The first six molecular orbitals (HOMO and LUMO) calculated for **1-3** ions. The most prominent MOs involved in the transitions under the lower energy band are highlighted.

are mostly composed of the Mn^I *d* orbitals and oxygen *p* orbitals, whereas the lowest unoccupied molecular orbital (LUMOs), which have a higher degree of delocalization, are composed of π^* Mn–CO and $p\pi^*$ nitrogen orbitals.

The HOMO energy values show the following trend: **1** > **3** > **2**, which is in agreement with the increase in the number of carbons attached to nitrogen atoms, directly influencing the σ -donating capabilities of the tridentate ligands. However, the LUMO energies value do not follow the same trend, showing a shift in the stabilization on comparing compounds **1** and **3**, resulting in band gap values of 5.49, 5.43 and 5.64 eV for **1**, **2** and **3**, respectively. Another key feature that appears when analyzing the calculated molecular orbitals (MOs) is that the increased symmetry from the tacn ligand imposes a higher degeneracy of the bonding MOs.

Correlations between the electronic spectra and the redox potentials for **1-3** were observed. The cyclic voltammograms for the three compounds in acetonitrile show two irreversible processes: the first at 624, 621 and 630 mV (*vs.* normal hydrogen electrode (NHE)) and the second at 1266, 1267 and 1265 mV (*vs.* NHE), for **1**, **2** and **3**, respectively. The first and second processes are attributed to the redox pairs Mn^I \rightleftharpoons Mn^{II} and Mn^{II} \rightleftharpoons Mn^{III}, respectively (Figures S8-S10, SI section). The high oxidation potentials of the manganese centers are due to the presence of the strong π acceptor CO groups, which decreases the electronic density on the metal, hindering the stabilization of higher oxidation states.

On changing the oxidation state of the manganese centers in the molecules there is a tendency for the CO from the first coordination to be replaced with solvent molecules, causing a strong change in the conformation of the compounds and influencing the reversibility of the processes. A lower intensity signal in the voltammograms for each compound can be observed close to the Mn^{II} \rightleftharpoons Mn^{III} oxidation potentials. This can be attributed to conformational changes due to the CO release during the oxidation process, which could either be attributed to the exchange of ligands or changes in the spin multiplicity. Unfortunately, the redox potential of this type of compound has not been widely studied, however, these properties are discussed in higher depth in the section related to the mechanistic processes involved in the photorelease of CO.

Considering the fact that the compounds **1-3** are diamagnetic, it was possible to perform NMR experiments in solution. In the ¹H NMR analysis results (Figure S11, SI section), compounds **1** and **2** show similar spectral profiles, where all of the methyl and methylene groups can be clearly observed. For compound **3**, the spectrum obtained was quite different, showing only a methylene group in its structure

and thus revealing a more symmetrical structure. Some of the resonance lines are broader and their magnetic splitting is altered due to the structural rigidity of the ligand imposed by the complexation process. Finally, primary (4.54 and 5.05 ppm for **1** and **2**, respectively) and secondary (6.24 and 6.71 ppm for **1** and **3**, respectively) amine hydrogen atoms were easily detected.

The ¹³C NMR spectra (Figure S12, SI section) of compounds **1** and **2** show similar features, except for the resonance line at 70.6 ppm in the spectrum of **2**, corresponding to the *N*-methyl group, which is absent from the spectrum of **1**. Once again, **3** reveals only one signal at 49.7 ppm, confirming its symmetrical ligand characteristic. All compounds show signals at around 220 ppm, attributed to the carbonyl groups attached to the manganese center. These ¹³C chemical shifts for the CO groups are in agreement with results for similar compounds described previously.³⁶

Photoactivated CO-release properties

In order to understand the photorelease behavior of the compounds **1-3** different wavelength light sources were tested, and the value of 385 nm was chosen because it leads to the most efficient photorelease and is very close to the calculated maximum wavelength for these compounds.

The changes in the CO stretching bands of compounds **1-3** upon exposure to λ_{385} was monitored by IR spectroscopy (Figure 5). As expected, after light exposure, the CO stretching bands located between 2050 to 1900 cm⁻¹ showed a steady decrease in intensity, until virtually disappearing after 1 h, indicating complete release from **1-3**, in agreement with the hemoglobin assay.

Besides noting the absence of the CO stretching bands after light exposure, the appearance of new lower intensity bands at lower frequencies was observed after 6 min of irradiation. These new bands are associated with the formation of biscarbonyl intermediates, which show CO stretching bands between 1950-1800 cm⁻¹, as also noted by Kurz's research group.^{30,31} This is in agreement with the CO stretching frequencies calculated for the intermediates, using DFT and the CPCM solvation model, exchanging the carbonyl ligand for an acetonitrile molecule (Table S1, SI section). The calculations indicate that all intermediates show one symmetric CO stretching band at around 1990 to 1960 cm⁻¹, which should be superposed by the asymmetric bands of the initial compounds, but this could not be observed during the photolysis experiments. The second CO stretching band at around 1900 to 1850 cm⁻¹, which appears in the photolysis experiments, is attributed to the asymmetric mode and confirmed by the theoretical values.

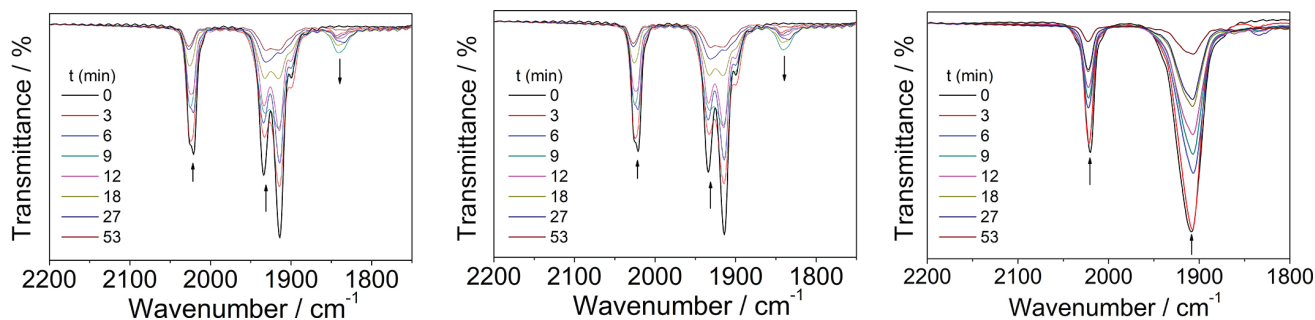


Figure 5. Changes in the infrared spectra (KBr) of **1** (left), **2** (middle) and **3** (right) caused by CO released during λ_{385} excitation, in acetonitrile solution.

The presence of these new bands is more evident for **1** and **2**, showing that for these compounds there is a buildup of the intermediate with two CO units. In contrast compound **3** does not show an increase in the intermediate concentration over time. This indicates that, after the excitation, the mechanisms involved in the release of carbon monoxide from compounds **1** and **2** are similar, while **3** readily loses the two remaining carbonyls after the first dissociation. Based on a comparison of the theoretical and experimental frequencies we propose that the intermediates biscarbonyl **1** and **2** are formed by the release of the carbonyl group *trans* to the NH_2 group of the aaz and Me_2aaz ligands.

The stability of the intermediates formed during the photodecomposition of **1** and **2** were also monitored in the absence of light, and in both cases the intermediates show only minor modifications of the CO stretching bands.

Analysis of the photoproducts by square wave voltammetry (Figure S13, SI section) demonstrated that after 6 min of light exposure, **1** and **2** show a new process at 0.383 and 0.493 V vs. NHE, respectively, attributed to the biscarbonyl intermediate, which does not change in the absence of light for 30 min. Overall, for both compounds, the manganese oxidation process continues for some time after the formation of the intermediates, with the modification of the potentials. However, when re-exposing the solutions to light, the initial species and the intermediates tend to lose the remainder of the CO and oxidize, lowering the intensity of the processes. A similar behavior was observed

by Kurz and co-workers³¹ for $[\text{Mn}(\text{CO})_3(\text{tpm})][\text{PF}_6]$. In this case, during cyclic voltammetry, the process occurred after 30 min of light (λ_{365} nm) exposure, with the appearance of a signal at 0.050 V vs. Fc/Fc^+ , attributed to oxidation of the intermediate $[\text{Mn}(\text{CO})_2(\text{tpm})(\text{CH}_3\text{CN})]^+$. This low oxidation potential of the biscarbonyl intermediate is due to the presence of only two strong π -accepting CO ligands, which increases the electron density on the Mn^{II} metal center, facilitating its oxidation.³¹

In contrast, when **3** (Figure S13, right, SI section) was exposed to light for 6 min, two processes appear: one at 0.423 V and the other at 0.655 V vs. NHE, both probably associated with the biscarbonyl species. However, in the absence of light, after 30 min, the stability of the intermediate formed decreases, probably due to auto-oxidation of the species formed at 0.332 V, which readily loses the other two carbonyls after the first dissociation.

In addition, the ESI-MS of the photoproducts (Figure 6) revealed that the compounds release only one CO molecule after 6 min of exposure to λ_{385} , exchanging the carbonyl group for a solvent molecule and retaining the Mn^{I} center, displaying peaks at 281.08 for **1** and **3** and 309.27 for **2**. This is coherent with the mechanism proposed by Kurz's research group.^{30,31} Unfortunately, during the analysis no other species resulting from the oxidation of the metal center were detected in appreciable amounts, even with longer exposures.

In order to determine the rates of the CO photorelease, the decomposition of **1-3** upon light irradiation were monitored

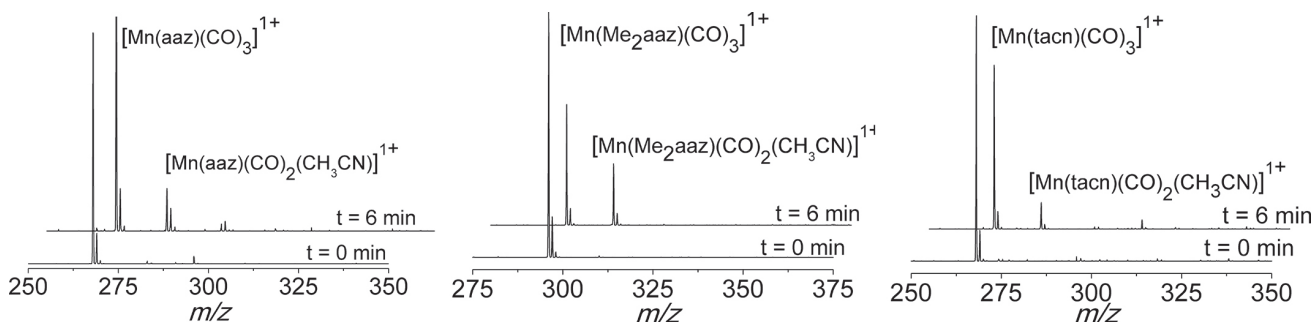


Figure 6. ESI-MS of **1-3** (from left to right) without irradiation and after 6 min of irradiation with λ_{385} .

spectrophotometrically over time in both optimum wavelengths ($\lambda_{385} = 385 \pm 10$ nm and $\lambda_{410} = 410 \pm 5$ nm), in order to infer whether there is a significant change in the photorelease rates.

Since, during the CO release experiment, **1-3** form a biscarbonyl species after about 6 min, the decay rates of the initial species was considered up to this time, disregarding the influence of the intermediate on the calculated rate. Moreover, the quantum yield was also determined using the ferrioxalate actinometry assay¹⁹ to determine the photon flux of the light sources used, using the same time interval.

The title compounds only showed some degree of decomposition when exposed to UV-A/violet light, with λ_{385} (calculated photon flux = 1.13×10^{-8} Einstein s⁻¹) and λ_{410} (calculated photon flux = 1.03×10^{-8} Einstein s⁻¹), respectively. At these wavelengths a decrease in the band centered at around 350 nm was observed until their stabilization around 16 and 36 min for λ_{385} and λ_{410} , respectively, when the solutions had a clear brown/yellow color. Figure 7 illustrates this behavior for complex **2**, while spectral data for complexes **1** and **3** are provided in Figures S14-S17 (SI section).

The results show that the decay rate and the quantum yields are directly proportional and that the CO release processes are faster during exposure to λ_{385} , in which all compounds showed higher quantum yield values compared to those found for λ_{410} exposure. These data are consistent with the absorption spectra and the calculated electronic transitions, which showed a strong absorption band around 350 nm, where the first major electronic transitions are observed, which are much closer to the UV-A wavelength used. During exposure to λ_{385} light, compound **2** was more

active showing both a higher decay rate and quantum yield value, while the quantum yields for **1** and **3** were very similar (Table 2). This higher activity of **2** can be explained by the presence of two methyl groups, which increases the σ -donating capabilities of the ligand, similarly to the use of Br and PPh₃ coligands in the first coordination sphere,³⁷ increasing the maximum wavelength of the first major electronic transitions for compound **2**, which is then closer to the incident wavelength. On increasing the incident light wavelength to λ_{410} , all compounds showed incomplete CO release and, therefore, the decomposition rates are slower than with λ_{385} and very similar.

The CO release was also studied using hemoglobin as a CO detector.³⁵ To eliminate any doubt regarding the interference of sodium dithionite in the CO release activity, the spectra were obtained for **1-3** without light irradiation and did not reveal any change in the Q bands of hemoglobin. The solutions were then exposed to the λ_{385} wavelength at fixed time intervals and the formation of HbCO was monitored by the decrease in the Hb 557 nm band and the appearance of two new bands at 538 and 567 nm associated with the conversion from Hb to HbCO (Figures S18-S20, SI section).

Considering these results, it is plausible to propose that the excitation of compounds **1** and **2** in λ_{385} wavelength releases one carbon monoxide molecule, forming a stable intermediate that does not undergo spontaneous oxidation, retaining the Mn^{II} center, and further CO release is only accomplished by light exposure. On the other hand, upon release of the first carbon monoxide molecule from compound **3**, the intermediate is rapidly oxidized, releasing all three CO units consecutively.

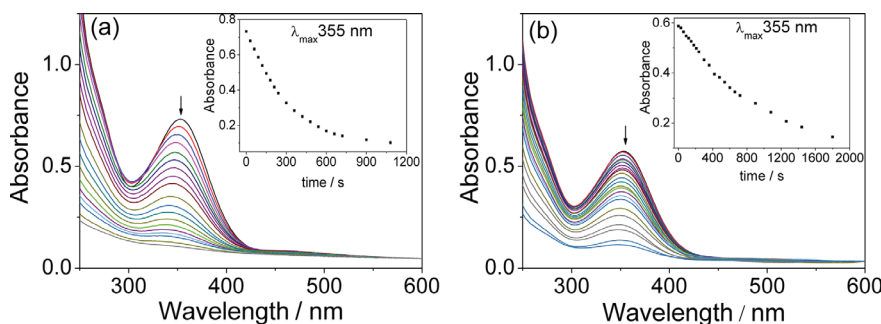


Figure 7. Changes in the UV-Vis spectra of a 1.0×10^{-3} mol L⁻¹ aqueous solution of compound **2** during the course of irradiation at (a) λ_{385} and (b) λ_{410} .

Table 2. Quantum yield of CO release for compounds **1-3** under irradiation at $\lambda_{385} = 385 \pm 10$ nm and $\lambda_{410} = 410 \pm 5$ nm

Compound	Quantum yield λ_{385}	Rate $_{\lambda_{385}} \times 10^{-7} / (\text{mol L}^{-1} \text{ s}^{-1})$	Quantum yield λ_{410}	Rate $_{\lambda_{410}} \times 10^{-7} / (\text{mol L}^{-1} \text{ s}^{-1})$
1	0.058 ± 0.008	6.65 ± 0.61	0.044 ± 0.003	4.48 ± 0.23
2	0.081 ± 0.002	9.10 ± 0.21	0.033 ± 0.003	3.17 ± 0.48
3	0.054 ± 0.002	5.97 ± 0.23	0.030 ± 0.001	3.06 ± 0.14

These proposed mechanisms are also in agreement with the quantum yield of CO release: quantum yield in λ_{385} $2 > 1 > 3$. In the case of compound **2**, the σ -donating capabilities of the methyl groups incorporated into the ligand seem to have a greater influence, whereas **1** and **3**, even though the excitation behaviors are similar, seem to be more influenced by the higher degree of oxidation after the release of the first CO. These results are consistent with those published by Kurz and co-workers.^{30,31}

When the photo-triggered CO release from the compounds **1-3** was studied via ^1H NMR, interesting features could be observed. The magnitudes of the quantum yield of CO release found by electronic spectroscopy (quantum yield in λ_{385} $2 > 1 > 3$) are reflected in the NMR spectral changes over time. Figure 8 illustrates this behavior for complex **2** while the results for complexes **1** and **3** are provided in the Supplementary Information (Figures S21 and S22, respectively).

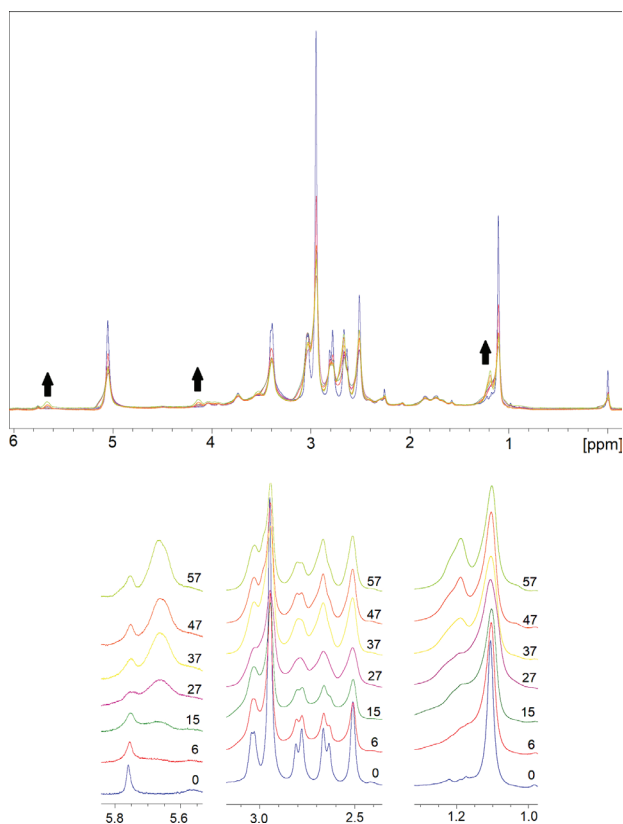


Figure 8. ^1H NMR spectral modifications for **2** (400 MHz, $\text{DMSO-}d_6$) upon irradiation with λ_{385} light. Full spectrum (top) and selected expansions (bottom). Time intervals: 0, 6, 16, 27, 37, 47, and 57 min.

Qualitatively, for all compounds, several new signals appeared on the ^1H spectra between 4.0 and 6.0 ppm after around 50 min of light exposure. This result could be related to the carbonyl dissociation with a concomitant solvent coordination ($\text{DMSO-}d_6$), generating new species

in solution. Considering the proximity of the nitrogen-attached protons (NH) of primary and secondary amines to the metal center, they can experience major shielding effects caused by the exchange of the exogenous ligands. Thus, more NH bonds are present in the compounds, as more new resonance lines appeared, over time. Considering the region between 1.0 and 4.0 ppm (methyl and methylene groups), all compounds showed smaller modifications, since these groups are distant from the manganese center. Interestingly, for **1** and **2**, the singlet at around 1.0 ppm (CH_3 group attached to the quaternary carbon of aaz and aaz- Me_2 ligands, respectively) presented the same effect observed for the amine protons mentioned above. In the case of compound **1**, two new singlets were detected, which may indicate new species generated in solution (Figure S21, SI section). The same trend can be observed for **2** (Figure 8); however, it is less pronounced since the carbonyl release is faster compared with **1** and thus less detectable.

On the ^{13}C spectra for **1-3** (Figures S23-S25, SI section), very elucidative features could be noted. For all compounds, when the spectra were taken before light exposure, a signal at around 220 ppm was detected, which relates to the manganese-bonded carbonyl group. After light exposure (around 50 min) a new resonance line is detected for all compounds between 180 and 190 ppm, attributed to the free carbonyl group in solution. This feature is in agreement with results obtained using other techniques, such as electrochemistry and mass spectrometry. Finally, for all resonance lines ascribed to the macrocyclic ligands (between 20 and 70 ppm), after light exposure new signals appeared around each line, which confirms the presence of different species in solution.

Based on these results a CO-release mechanism can be proposed for compounds **1-3** (Figure 9), which consists of two steps. After approximately 6 min of light exposure, all compounds release one equivalent of CO resulting in a biscarbonyl species with a solvent molecule replacing the CO released. This is confirmed by the ESI-MS, IR, and NMR spectroscopy results. At this point the compounds could be separated into two groups. For the first group, containing compounds **1** and **2**, we propose that after the release of the first CO the two remaining CO molecules are released after longer exposure to light with subsequent oxidation of the metal center (from Mn^{I} to Mn^{II}). This is corroborated by the IR spectra, which show that the new signals attributed to the biscarbonyl intermediate disappear after longer exposure to light (Figure 5). In addition, the signals relating to CO stretching in the starting compounds disappear completely, verifying the release of all CO molecules. For the second group (compound **3**), we propose that after the first 6 min under light exposure simultaneously

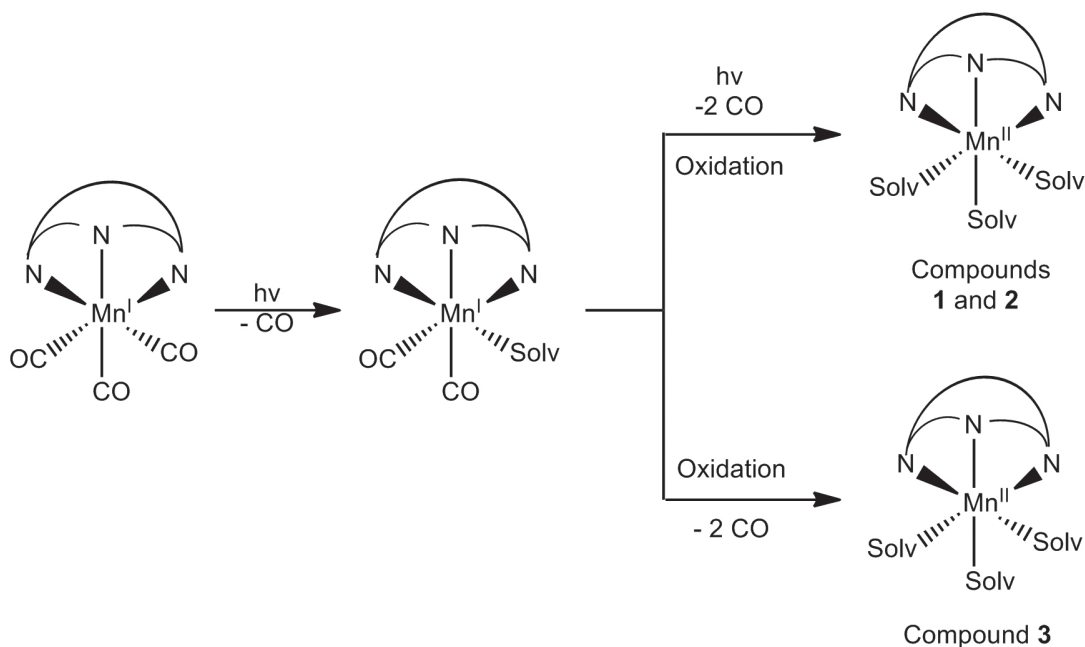


Figure 9. Proposed schematic representation of the CO release for 1-3.

occur the oxidation of the metal center (Mn^I/Mn^{II}) and the release of the two remaining CO molecules. This is corroborated by the IR spectrum for this compound, which does not show the appearance of a new signal relating to the bis-carbonyl intermediate. However, this new signal does appear on the mass spectrum. This suggests that, for compound **3**, this intermediate is unstable leading to rapid oxidation of the metal center with the subsequent release of the other two CO molecules after a longer exposure to light, which is evidenced by the disappearance of the bands associated with the CO stretching in the IR spectrum. Regarding compounds **1** and **2**, the oxidation of the metal center can be confirmed by the ¹H NMR results, where the resonance lines become broad, indicating the paramagnetism of the Mn^{II} metal center. Some researchers suggest the dimerization of the metal centers after the release of the CO molecules,^{30,31} but our results did not confirm this.

Conclusions

Three water-soluble Mn^I tricarbonyl compounds with the cyclic ligands aaz, Me₂aaz and tacn were synthesized. The compounds released CO molecules when exposed to light (λ_{385} and λ_{410}), thus acting as photoCORMs. Excitation at a wavelength of λ_{385} caused the fastest CO release for all compounds and **2** had the faster CO release under this condition. Using the combined techniques of IR, UV-Vis and NMR spectroscopies, along with ESI-MS and electrochemistry, it was possible to identify the formation

of a bis-carbonyl intermediate for all compounds during the photo-release process. On applying the hemoglobin assay for 95 min using light at λ_{385} , the compounds showed CO release and we did not observe an influence of sodium dithionite in this process. The CO release appears to occur in two steps, as shown in Figure 9 with compounds **1** and **2** exhibiting a slightly different mechanism compared with compound **3**.

Supplementary Information

Crystallographic data (excluding structure factors) for the structures in this work were deposited in the Cambridge Crystallographic Data Centre as supplementary publication number CCDC 1892760-1892762. Copies of the data can be obtained, free of charge, via www.ccdc.cam.ac.uk/conts/retrieving.html or from the Cambridge Crystallographic Data Centre, CCDC, 12 Union Road, Cambridge CB2 1EZ, UK; fax: +44 1223 336033. E-mail: deposit@ccdc.cam.ac.uk.

Supplementary information (NMR spectra, IR spectra, UV spectra, electrochemical studies, mass spectra) is available free of charge at <http://jbcs.sbq.org.br> as a PDF file.

Acknowledgments

The authors are grateful to the Brazilian governmental agencies CNPq (for grants awarded to A. N., A. J. B., A. L. A. and R. A. P.) and to IFSC, INCT-Catálise and FINEP.

This study was financed in part by the Coordenação de Aperfeiçoamento de Pessoal de Nível Superior, Brasil (CAPES), Finance Code 001.

References

1. Foresti, R.; Bani-Hani, M. G.; Motterlini R.; *Intensive Care Med.* **2008**, *34*, 649.
2. Motterlini, R.; Otterbein, L. E.; *Nat. Rev. Drug Discovery* **2010**, *9*, 728.
3. Kim, H. P.; Ryter, S. W.; Choi, A. M.; *Annu. Rev. Pharmacol. Toxicol.* **2006**, *46*, 411.
4. Fukuto, J. M.; Carrington, S. J.; Tantillo, D. J.; Harrison, J. G.; Ignarro, L. J.; Freeman, B. A.; Chen, A.; Wink, D. A.; *Chem. Res. Toxicol.* **2012**, *25*, 769.
5. Otterbein, L. E.; Bach, F. H.; Alam, J.; Soares, M.; Lu, H. T.; Wysk, M.; Davis, R. J.; Flavell, R. A.; Choi, A. M.; *Nat. Med.* **2000**, *6*, 422.
6. Mann, B. E.; Motterlini, R.; *Chem. Commun.* **2007**, *45*, 4818.
7. Ryter, S. W.; Choi, A. M. K.; *Am. J. Respir. Cell Mol. Biol.* **2009**, *41*, 251.
8. Blumenthal, I.; *J. R. Soc. Med.* **2001**, *94*, 270.
9. Garcia-Gallego, S.; Bernardes, G. J. L.; *Angew. Chem., Int. Ed.* **2014**, *53*, 9712.
10. Bauer, I.; Pannen, B. H.; *Crit. Care* **2009**, *13*, 220.
11. Mann, B. E.; *Organometallics* **2012**, *31*, 5728.
12. Romão, C. C.; Blättler, W. A.; Seixas, J. D.; Bernardes, G. J. L.; *Chem. Soc. Rev.* **2012**, *41*, 3571.
13. Schatzschneider, U.; *Br. J. Pharmacol.* **2015**, *172*, 1638.
14. Fris, S. D.; Taaning, R. H.; Lindhardt, A. T.; Skrydstrup, T.; *J. Am. Chem. Soc.* **2011**, *133*, 18114.
15. Antony, L. A. P.; Slanina, T.; Sebej, P.; Solomek, T.; Klán, P.; *Org. Lett.* **2013**, *15*, 4552.
16. Rimmer, R. D.; Richter, H.; Ford, P. C.; *Inorg. Chem.* **2010**, *49*, 1180.
17. Seixas, J. D.; Mukhopadhyay, A.; Santos-Silva, T.; Otterbein, L. E.; Gallo, D. J.; Rodrigues, S. S.; Guerreiro, B. H.; Gonçalves, A. M. L.; Penacho, N.; Marques, A. R.; Coelho, A. C.; Reis, P. M.; Romão, M. J.; Romão, C. C.; *Dalton Trans.* **2013**, *42*, 5985.
18. Romanski, S.; Rucker, H.; Stamellou, E.; Guttentag, M.; Neudorfl, J.-M.; Alberto, R.; Amslinger, S.; Yard, B.; Schmalz, H.-G.; *Organometallics* **2012**, *31*, 5800.
19. Bischof, C.; Joshi, T.; Dimri, A.; Spiccia, L.; Schatzschneider, U.; *Inorg. Chem.* **2013**, *52*, 9297.
20. Pierri, A. E.; Pallaoro, A.; Wu, G.; Ford, P. C.; *J. Am. Chem. Soc.* **2012**, *134*, 18197.
21. Jimenez, J.; Chakraborty, I.; Mascharak, P. K.; *Eur. J. Inorg. Chem.* **2015**, *30*, 5021.
22. Clark, J. E.; Naughton, P.; Shurey, S.; Green, C. J.; Johnson, T. R.; Mann, B. E.; Foresti, R.; Motterlini, R.; *Circ. Res.* **2003**, *93*, e2.
23. Chakraborty, I.; Carrington, S. J.; Roseman, G.; Mascharak, P. K.; *Inorg. Chem.* **2017**, *56*, 1534.
24. Johnson, T. R.; Mann, B. E.; Teasdale, I. P.; Adams, H.; Foresti, R.; Green, C. J.; Motterlini, R.; *Dalton Trans.* **2007**, 1500.
25. Rimmer, R. D.; Pierri, A. E.; Ford, P. C.; *Coord. Chem. Rev.* **2012**, *256*, 1509.
26. Wright, M. A.; Wright, J. A.; *Dalton Trans.* **2016**, *45*, 6801.
27. Motterlini, R.; Clark, J. E.; Foresti, R.; Sarathchandra, P.; Mann, B. E.; Green, C. J.; *Circ. Res.* **2002**, *90*, e17.
28. Meister, K.; Niesel, J.; Schatzschneider, U.; Schmidt, D. A.; Metzler-Nolte, N.; Havenith, M.; *Angew. Chem., Int. Ed.* **2010**, *49*, 3310.
29. Jimenez, J.; Chakraborty, I.; Dominguez, A.; Martinez-Gonzalez, J.; Sameera, W. M. C.; Mascharak, P. K.; *Inorg. Chem.* **2018**, *57*, 1766.
30. Berends, H. M.; Kurz, P.; *Inorg. Chim. Acta* **2011**, *380*, 141.
31. Sachs, U.; Schaper, G.; Winkler, D.; Kratzert, D.; Kurz, P.; *Dalton Trans.* **2016**, *45*, 17464.
32. Aime, S.; Calabi, L.; Cavallotti, C.; Gianolio, E.; Giovenzana, B. G.; Losi, P.; Maiocchi, A.; Palmisano, G.; Sisti, M.; *Inorg. Chem.* **2004**, *43*, 7588.
33. Appel, M. A. C.; Hagel, R.; Russel, W. S.; Tetard, D.; *WO pat. 01/85717 A1* **2001**.
34. Gagne, R. R.; Koval, C. A.; Lisensky, G. C.; *Inorg. Chem.* **1980**, *19*, 2854.
35. Atkin, A. J.; Lynam, J. M.; Moulton, B. E.; Sawle, P.; Motterlini, R.; Boyle, N. M.; Pryce, M. T.; Fairlamb, I. J. S.; *Dalton Trans.* **2011**, *40*, 5755.
36. Mede, R.; Hoffmann, P.; Klein, M.; Görls, H.; Schmitt, M.; Neugebauer, U.; Gessner, G.; Heinemann, H. S.; Popp, J.; Westerhausen, M.; *Z. Anorg. Allg. Chem.* **2017**, *643*, 2057.
37. Chakraborty, I.; Carrington, S. J.; Mascharak, P. K.; *Acc. Chem. Res.* **2014**, *47*, 2603.

Submitted: April 21, 2019

Published online: August 6, 2019

